Journal of Photochemistry & Photobiology A: Chemistry 401 (2020) 112778

Contents lists available at ScienceDirect

Journal of Photochemistry & Photobiology A: Chemistry

journal homepage: www.elsevier.com/locate/jphotochem

Improved photoelectrocatalytic properties of ZnO/$CuWO_4$ heterojunction film for RhB degradation

João P.C. Moura[a], Roberta Y.N. Reis[b], Aline E.B. Lima[a], Reginaldo S. Santos[a,b], Geraldo E. Luz Jr[a,b,*]

[a] PPGQ-DQ-Universidade Federal do Piauí, Teresina, PI, CEP – 64049550 Brazil
[b] PPGQ-GERATEC-DQ-Universidade Estadual do Piauí, Rua: João Cabral, N. 2231, P.O. Box 381, 64002-150, Teresina, PI, Brazil

ARTICLE INFO

Keywords:
Heterojunction
ZnO/CuWO4
ZnO nanorods
Photoelectrocatalysis
Electro assisted photocatalysis

ABSTRACT

In this work, we report on the photoelectrocatalytic properties of nanostructured ZnO/$CuWO_4$ heterojunction film prepared by combining the hydrothermal and doctor-blade methods. For ZnO and $CuWO_4$ heterojunction films, X-ray diffraction (XRD) spectra showed the wurtzite and triclinic structure phases, respectively, and no deleterious phases were observed. Scanning electron microscopy (SEM) images showed ZnO nanorods (NRs) grown perpendicular to the substrate and a $CuWO_4$ nanoparticle surface coating on the ZnO/$CuWO_4$ film. The formation of heterojunction film allowed a greater use of visible light and better photoelectrochemical behavior for the ZnO/$CuWO_4$ film. The ZnO, $CuWO_4$, and ZnO/$CuWO_4$ films were used for electrochemically assisted (PEC) RhB photodegradation. The ZnO/$CuWO_4$ film had a PEC photodegradation efficiency of 82 %, making it approximately twice as effective as ZnO film. The incorporation of $CuWO_4$ into the ZnO NR array film with a bias potential remarkably promoted the photogenerated carrier separation and increased the use of photogenerated carriers in photocatalytic reactions, resulting in a higher photocatalytic activity under visible light.

1. Introduction

The semiconductor heterojunction systems have attracted research interest in recent years due to novel properties that make them suitable for application, especially in photocatalysis for environmental water remediation, water splitting to produce clean hydrogen fuel, and photovoltaic devices [1]. Heterojunction formation involves the combination of two or more semiconductors to form new materials with superior electrical, optical, and catalytic properties due to transfer of the interfacial charge and a synergistic effect between coupled semiconductors [2].

Many semiconductor materials have been investigated, such as the binary oxides, TiO_2 [3], ZnO [4] and CuO [5], and the complex oxides: $CuWO_4$ [6], $BiVO_4$ [7], and $LaFeO_3$ [8]. The selection of a semiconductor catalyst for efficient activity depends on properties such as adequate band gap energy, good stability, high carrier mobility, the correct band-edge position, and efficient light absorption [9]. The formation of an appropriated heterojunction can result in properties that overcome the intrinsic drawbacks of the use of a single catalyst [10].

In this context, zinc oxide (ZnO) has been widely studied for use as a photocatalyst in optoelectronic devices and solar cells due to its physical properties, high catalytic activity, environmental sustainability, synthetic facility, high electronic mobility, and high thermal conductivity [11,12]. ZnO is also advantageous because it can be obtained in a wide variety of nanostructures such as nanoparticles [13], core-shell nanoparticles [14], hierarchical structures [15], nanoflowers [16], nanosheets [17], vertically aligned nanowires [18], nanorods [4], and nanotubes [19], which can directly alter material properties. Despite its many advantages, ZnO has a wide band gap energy (E_{bg}) of approximately 3.2 eV, which limits its absorption of solar radiation to the ultraviolet region (approximately 3%–5% of total solar energy), and it has a high recombination rate of photogenerated loads. In addition, it undergoes photocorrosion and is soluble in acidic and basic media. These drawbacks make pure ZnO an unattractive choice as a photocatalyst under visible light [9].

ZnO-based heterojunction strategies can be adopted to improve the optical, photoelectrochemical, and photocatalytic properties as well as the stability. Several studies have investigated the ZnO heterojunction with oxide catalysts such as ZnO/CuO [20], ZnO/Fe_2O_3 [21], ZnO/WO_3 [22], and ZnO/$BiVO_4$ [23], and these heterojunctions exhibited improved photocatalytic activity (mainly derived from the prolonged lifetime of the photoexcited e^-/h^+ pairs), enhanced transfer of the

* Corresponding author at: PPGQ-DQ-Universidade Federal do Piauí, Teresina, PI, CEP – 64049550 Brazil.
E-mail address: geraldoeduardo@ccn.uespi.br (G.E. Luz).

https://doi.org/10.1016/j.jphotochem.2020.112778
Received 13 February 2020; Received in revised form 26 May 2020; Accepted 12 July 2020
Available online 13 July 2020
1010-6030/

interfacial charge, greater photostability, and expansion of the absorption spectrum to the visible range [2,9].

Copper tungstate ($CuWO_4$) has recently attracted attention in the scientific community due its narrow band gap energy, chemical stability, and photocatalytic activity in photoelectrochemical (PEC) water splitting and the degradation of organic pollutants [24–26]. $CuWO_4$ has an E_{bg} ranging from 2.0 to 2.4 eV and is therefore a semiconductor that can absorb visible radiation [27,28]. Despite these inherent advantages, the application of $CuWO_4$ remains hampered due to drawbacks such as a low transfer speed and a high recombination rate of charge carriers [29]. To overcome some of the disadvantages presented by many semiconductors and increase their photocatalytic efficiency, oxides supported in film form (photoelectrode) have been used. In semiconductor electrode films, it is possible to apply a bias potential, which can promote a reduction of electron–hole pair (e^-/h^+) recombination [30–32]. The investigations of $ZnO/CuWO_4$ heterostructure are recent and the works report only the study of powder composites. [33,34].

Therefore, to improve the chemical stability and optical properties of ZnO, in this work we prepared a heterojunction film by coating ZnO nanorods with $CuWO_4$ nanoparticles deposited on a fluoride-doped tin oxide (FTO) glass substrate. In addition, we determined the optical, structural, morphological, and photoelectrochemical properties of the film. Furthermore, the synergetic effects in charge transport, stability, and application to photocatalysis was investigated using rhodamine B as a model pollutant under polychromatic irradiation.

2. Experimental details

2.1. Chemicals

Zinc acetate dihydrate ($Zn(C_2H_3O_2)_2\ 2H_2O \geq 99.0$ %), 2-methoxyethanol ($C_3H_8O_2 \geq 99.8$ %), zinc nitrate hexahydrate ($Zn(NO_3)_2\ 6H_2O \geq 99.0$ %), cupric nitrate trihydrate ($Cu(NO_3)_2\ 3H_2O \geq 99$ %–104 %), sodium tungstate dihydrate ($Na_2WO_4\ 2H_2O \geq 99$ %), and rhodamine B (RhB ~ 95 %) were purchased from Sigma Aldrich. 2-Aminoethanol (MEA ≥ 99 %), sodium sulfate ($Na_2SO_4 \geq 99.0$ %), and hexamethylenetetramine (HMTA ≥ 99.5 %) were purchased from Dinâmica. Glass fluorine-doped tin oxide–FTO (SnO:F, sheet resistance 8 Ω/sq) was purchased from Aliyiqi. Deionized water was used in all experiments. All chemicals were of purely analytical grade and were used without any further purification.

2.2. Preparation of ZnO nanorod films

FTO glass (with the dimensions of 2.5 cm × 1 cm) was used as the substrate for all films. The FTO was cleaned in an ultrasonic batch first with neutral detergent and water, and then with water and isopropyl alcohol. The area of all prepared films was 1 cm^2.

ZnO nanorod array films were prepared following the typical two-step methodology [35]. First, a seed layer was deposited onto the FTO substrate using the spin coating method. A seed layer solution consisting of a sol-gel solution of 0.5 M $Zn(Ac)_2$ in 2-methoxethanol solvent with the MEA stabilizer (mole ratio 1:1 Zn^{2+}/MEA) was prepared. The seed layer solution was dropped onto a glass substrate, which was rotated at 1000 rpm for 30 s, and the spin-deposition was repeated three times, with the sample heated at 200 °C for 20 min between each deposition. After the deposition, the film was heated in a furnace at 500 °C for 60 min at 2 °C min^{-1}. The precursor solution for nanorod growth was an equimolar (25 mM) mixture of aqueous solutions of $Zn(NO_3)_2$ and HMTA. The film with the seed layer was vertically immersed in this solution in a glass bottle, sealed, and then heated at 95 °C for 8 h. Finally, the film was rinsed with deionized water, dried in atmospheric conditions, and then treated at 500 °C for 60 min at 2 °C min^{-1}.

2.3. Synthesis of the $CuWO_4$ electrode film and heterojunction electrode preparation

$CuWO_4$ was synthesized using the co-precipitation method followed by hydrothermal treatment, and the $CuWO_4$ electrodes were prepared using the doctor-blade method reported by Lima et al. [36]. Briefly, 2 mmol of $CuNO_3$ and Na_2WO_4 precursor solutions were transferred to the same beaker and sonicated for 10 min, allowed to rest for 48 h, and then the resulting suspension was washed in a centrifuge to remove ions. Then, the suspension was transferred to an autoclave with a Teflon inner container, sealed and heated at 200 °C for 8 h. For preparation of the $CuWO_4$ electrode, a 25-μL aliquot of the $CuWO_4$ suspension was deposited onto FTO using the doctor- blade method, dried at room temperature (repeated two times) and heated at 500 °C for 30 min at 2 °C min^{-1}. For the preparation of $ZnO/CuWO_4$ heterojunction films, this same procedure was used but an aliquot of suspension was deposited onto previously prepared ZnO nanorod arrays and heated at 500 °C for 30 min at 2 °C min^{-1}.

2.4. Characterization of films

The crystalline structure was analyzed using a D/MAX/2500PC diffractometer (Rigaku, Japan) operating at 40 kV and 150 mA with Cu Kα radiation ($\lambda = 1.5406$ Å) in the 2θ range of 10°–110° at a scan rate of 0.02°/min. The morphologic properties of the films were investigated using a field emission scanning electron microscope (Carl Zeiss, Model Supra 35-VP, Germany) operated at an accelerating voltage of 2 kV. The optical properties of the films were investigated using a UV–vis spectrophotometer Model UV-2600 (Shimadzu, Japan)

2.5. Photoelectrochemical studies and photocatalytic performance measurements

Photoelectrochemical analyses were conducted in a glass cell (100 % transmittance for $\lambda > 360$ nm) with three electrodes including the prepared films as the work electrode. A platinum wire was used as the counter electrode and Ag/AgCl (KCl sat.) was used as the reference electrode. A 0.1 M aqueous solution of Na_2SO_4 was used as an inert support electrolyte (pH = 5.6). The measurements were performed in a potentiostat/galvanostat (PGSTAT302 N Metrohm) under polychromatic irradiation from a metallic vapor discharge lamp (HQI-TS NDL) with a nominal potency of 150 W. Some measurements were taken in the absence of irradiation, which is named the dark condition. All measurements were performed at room temperature.

For comparison with the values reported in the literature, the potentials applied in the Ag/AgCl reference electrode were adjusted to that of a reversible hydrogen electrode (RHE) using Eq. (1) [37]:

$$(1)\ (RHE) = -E(Ag/AgCl) + 0.0591.\ pH + 0.199\ V$$

Further, the potentials adjusted with respect to the RHE (in volts) were converted to electron-volts (eV) using Eq. (2) [30]:

$$(2)\ (eV) = -4.5\ eV - eE(RHE)$$

The photocatalytic activity of the ZnO, $CuWO_4$, and $ZnO/CuWO_4$ film electrodes was investigated by degrading 17 ml of a 1×10^{-6} M solution of rhodamine B (RhB) dissolved in a 0.1 M aqueous solution of Na_2SO_4 as the support electrolyte. These studies were performed in the following three configures: (i) photolysis—irradiation of the solution without the photocatalyst, so that only the clean FTO substrate was used; (ii) photocatalysis (PC)—irradiating photocatalyst films; and (iii) electrochemically assisted photocatalysis (PEC)—the films were irradiated and polarized in a bias voltage of +0.7 V *vs* Ag/AgCl. The distance between the lamp and the photocatalysis cell was 10 cm. In the assays, the system was not stirred or heated. At regular time intervals, an aliquot of the solution was collected and analyzed with a UV/Vis

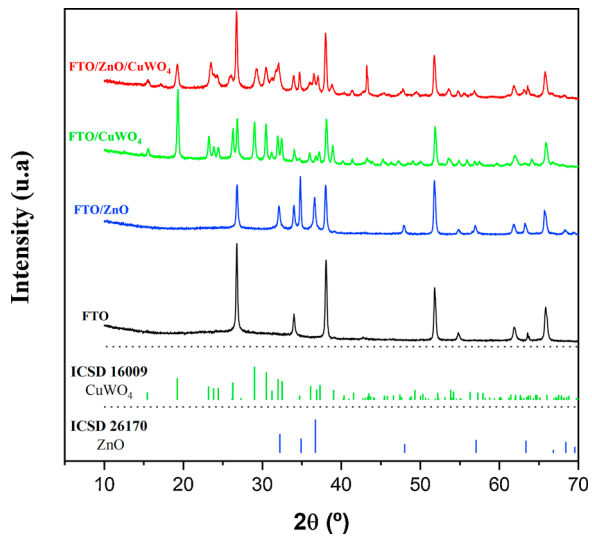

Fig. 1. XRD patterns for substrate FTO, ZnO, $CuWO_4$ and ZnO/$CuWO_4$ heterojunction films.

absorption spectrometer to determine the kinetic parameters and to monitor the relative variation of RhB concentration.

3. Results and discussion

3.1. Structural and morphological characterization

The phases and crystalline structure of the films were analyzed using X-ray diffraction (XRD) spectroscopy. Fig. 1 presents the XRD patterns of the ZnO, $CuWO_4$, and ZnO/$CuWO_4$ films as well as that of the FTO substrate. The peaks located at 2θ values of 26.7°, 33.8°, 38.1°, 51.9°, 54.8°, 61.9°, 63.3°, and 65.8° are present in all spectra and are related to the FTO glass conductive substrate. For the ZnO and $CuWO_4$ films, all peaks are in great agreement with the inorganic crystal structure data n° 26,170 (ZnO) and n° 16,009 ($CuWO_4$) [38,39], respectively, referring to the phases of the wurtzite zinc oxide and triclinic copper tungstate structures.

In the ZnO/$CuWO_4$ heterojunction XRD pattern, the peaks referring to the phases of $CuWO_4$ and ZnO are preserved, which proves the successful synthesis of the crystalline ZnO/$CuWO_4$ heterojunction.

SEM images for the top-view and cross-section view of deposited ZnO, $CuWO_4$ and ZnO/$CuWO_4$ films are shown in Fig. 2. The density of the mass deposited onto the FTO glass was 0.7 ± 0.1; 1.3 ± 0.3, and 2.4 ± 0.5 mg cm^{-3} (n = 6) for ZnO, $CuWO_4$ and ZnO/$CuWO_4$, respectively. All films showed a uniform recovery of the FTO-glass substrate. The top-view SEM images in Fig. 2a–b show that ZnO nanorods with an average diameter of 68 ± 9 nm grow perpendicularly from the substrate. The cross-section image (Fig. 2c) shows that the nanorods have a non-uniform length of approximately 3 μm.

Fig. 2d–f show the $CuWO_4$ film SEM images. The top-view images (Fig. 2d–e) reveal films containing agglomerated, irregularly shaped grains with sizes of 98 ± 32 nm, whereas the cross-section image (Fig. 2f) shows that the thickness of the film is 1.20 μm.

Fig. 2g–i exhibit SEM images of the heterojunction films formed by $CuWO_4$-layered ZnO nanorods. The layer of $CuWO_4$ thoroughly covers the top surface of the nanorods, whose morphology is maintained after formation of the ZnO/$CuWO_4$ heterostructure.

3.2. Optical characterization and estimate of the band gap energy

The transmittance UV–vis spectra and the Tauc plot for estimating the E_{bg} of the films are shown in Fig. 3. In Fig. 3a, the UV–vis spectrum of the ZnO film shows the characteristics of the UV–vis spectra of other ZnO films, with a high transmittance in the visible region and an abrupt termination near 400 nm; however, the ZnO/$CuWO_4$ heterojunction film presents absorption shifted to the visible region. Association of ZnO with a narrow gap semiconductor is a well-reported way to shift the absorbance to the visible region, suggesting facilitation of the effective separation of the photoexcitation charge carriers [21,33,40].

Optical band gap values were estimated from the transmittance UV–vis spectra using the Tauc method, according to Eq. 3 [41,42].

$$(\alpha h\nu)^n = A(h\nu - E_{bg}) \quad (3)$$

where α is the absorption coefficient, A is a constant, h is Planck's constant, ν is the photon frequency, E_{bg} is the optical band gap, and n is equal to 2 for a direct transition or 1/2 for an indirect transition; thus, the value of the indirect optical band gap of the $CuWO_4$ film is 2.08 eV, and that of the direct gap of the ZnO film is 3.22 eV, which agrees with the results of previously published studies [27,43]. The direct E_{bg} for ZnO/$CuWO_4$ is 2.19 eV, suggesting that $CuWO_4$ significantly expands the absorption of ZnO film to the visible region, and thus the ZnO/$CuWO_4$ film can produce electron–hole pairs under visible light irradiation [44].

3.3. Photoelectrochemical properties

The photocurrent response of ZnO, $CuWO_4$ and ZnO/$CuWO_4$ films, shown in Fig. 4, was investigated using cyclic voltammetry, linear voltammetry, and chronoamperometric analysis in 0.1 M of inert electrolyte Na_2SO_4 under polychromatic irradiation. The voltammetric responses displayed in Fig. 4a (dashed lines) present almost no current density in the absence of irradiation; however, when the semiconductors were irradiated, photoelectrons were excited from the valence band to the conducting band and a photocurrent was generated [35]. In addition, the photocurrent densities increased with the applied potential, suggesting that the potential could effectively drive the photogenerated electrons to the counter electrode, avoiding electron and hole pair recombination [45].

Fig. 4b–c show the photocurrent-time responses in chronoamperometric analysis at 0.7 V *vs* Ag/AgCl. All films present the n-type semiconductor behavior, exhibiting negative variations of the open-circuit potential after light irradiation. The ZnO/$CuWO_4$ heterojunction film presents the most photocurrent density among the investigated films. The enhancement in its anodic photocurrent can be attributed to a favorable alignment of the semiconductor energy band-edge positions that improves the mobility of the photogenerated charges and decreases electron–hole recombination [46]. In addition, the one-dimensional structure of the ZnO nanorod arrays can act as a directional charge transport path [47].

It is well known that ZnO is chemically unstable and undergoes photocorrosion [48]. Fig. 4c compares the results of a photostability test developed for the ZnO/CuWO4 photoelectrode with the results for ZnO film. The exponential decay of the photocurrent density is related to ZnO photocorrosion [49], which is induced by reaction with photogenerated holes (h_{VB}^+) according to the equation ZnO + $2h_{VB}^+ \rightarrow Zn^{2+}$ + ½ O_2 [50]. This analysis shows that the photostability of the ZnO/$CuWO_4$ film improved in comparison to that of pure ZnO film. The enhanced stability may be closely linked to the charge transport optimization of holes in the ZnO/$CuWO_4$ semiconductors, as such holes do not accumulate in the ZnO semiconductor.

The linear voltammogram anodic scans from −0.1 to 1.1 V *vs* Ag/AgCl, with a chopper irradiation of 0.1 Hz, are shown in Fig. 5a–b. The photocurrent density intensities recorded here agree with the results of cyclic voltammetry presented in Fig. 4. From these photoresponse measurements, it is possible to estimate the semiconductor flat band potential (Efb), which is related to the relative Fermi level [51]. The Efb was determined using the Buttler–Gartner model, according to Eq. 4 [52].

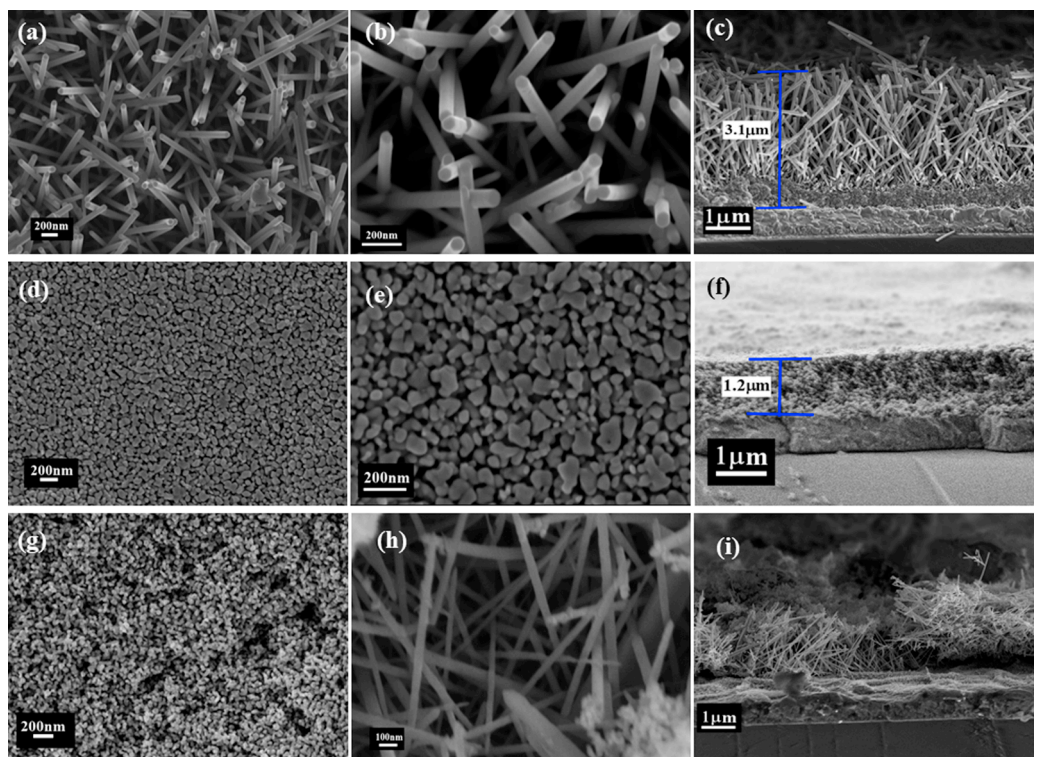

Fig. 2. SEM images for films (a-c) ZnO nanorods; (d-f) $CuWO_4$ and (g-i) $ZnO/CuWO_4$.

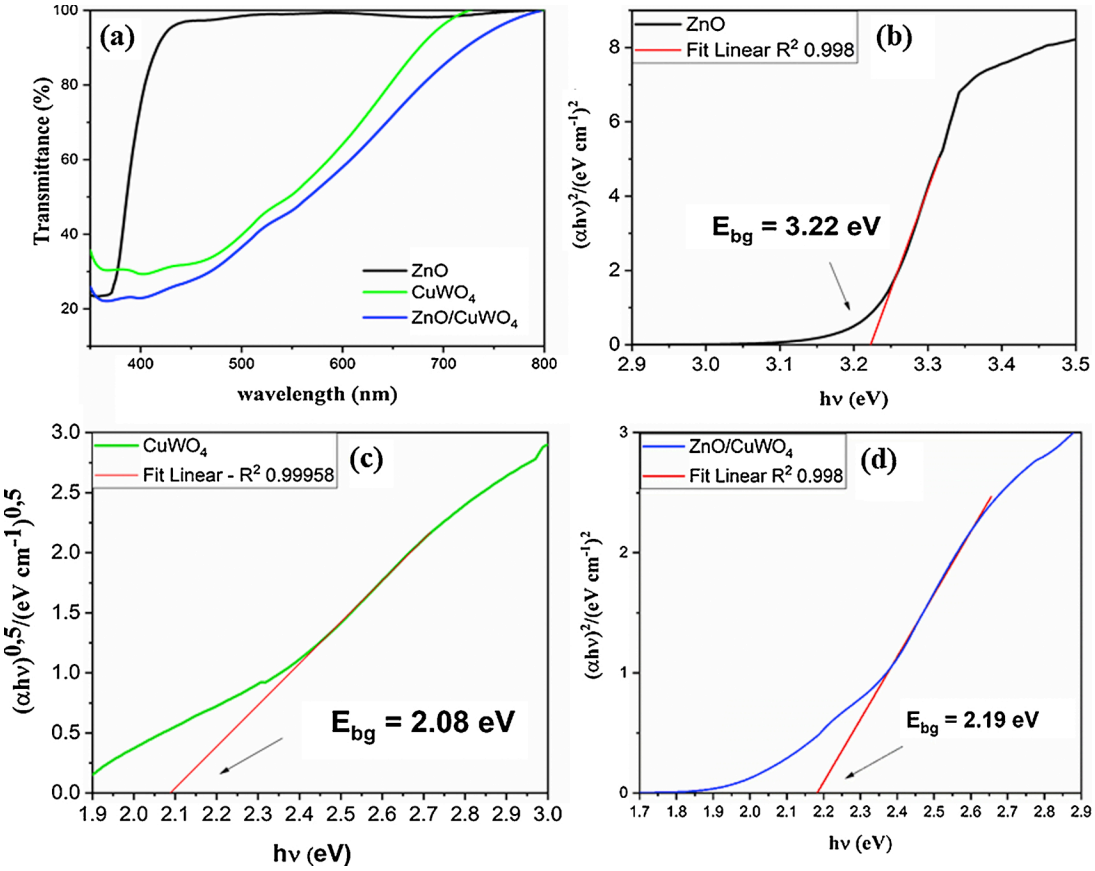

Fig. 3. (a) UV–vis transmittance spectra and corresponding Tauc plot of (b) ZnO, (c) $CuWO_4$ and (d) $ZnO/CuWO_4$ films.

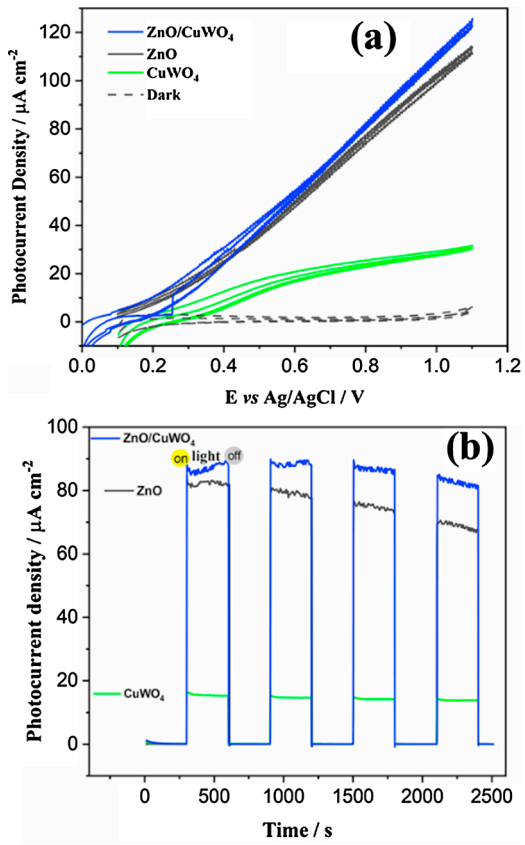

Fig. 4. (a) Cyclic voltammetry at scan rate 20 mV s^{-1} and (b-c) chronoamperometric curves under applied 0.7 V *vs* Ag/AgCl with polychromatic irradiation in 0.1 mol L^{-1} Na_2SO_4 aqueous solution.

$$I = \alpha W0 q \varphi 0 \sqrt{(E - Efb)} \quad (4)$$

where α is the absorption coefficient, *W*0 is the depletion layer, *φ*0 is the photon flux, *q* is the electron charge, and *E*fb is the flat band energy.

The estimated Efb values (inset of Fig. 5) are 0.02 and 0.16 V *vs* Ag/AgCl for ZnO and $CuWO_4$ films, respectively. For type-n semiconductors, Efb is a useful parameter because it is close in value to the conduction band (E_{BC}) potential [53]. By combining this result with the previously determined E_{bg}, it is possible to predict the band-edge potential alignment for all semiconductor materials in ZnO/$CuWO_4$ heterojunction film, as illustrated in Fig. 5d. Semiconductor heterojunction band alignments allow the transport of e^-/h^+ pair charges, which is favorable for decreasing the number of recombination and enhancing the photocurrent density.

The electrochemical behavior of RhB at the ZnO/$CuWO_4$ film photoanode, shown in Fig. 5c, exhibits no redox signals when 0.1 M Na_2SO_4 is used as a supporting electrolyte; however, in 1.0×10^{-6} M RhB solution, one oxidation peak is observed at 0.9 V *vs* Ag/AgCl, which is attributed to direct electro-oxidation of RhB [54,55]. Using this oxidation potential in Eq.s 1 and 2, a value of −6.03 eV is obtained for the energy of the highest occupied molecular orbital (HOMO) of RhB [56]. From an analysis of the UV–vis spectrum, it is possible to determine the energy gap between the HOMO and the lowest unoccupied molecular orbital (LUMO) [57]. Fig. 5c (inset) shows the optical absorption spectrum of an RhB solution in 0.1 M Na_2SO_4. The HOMO-LUMO energy difference may be estimated from the maximum dye absorbance of 553 nm using the following relationships: $Eg_{(eV)} = 1241/\lambda_{(nm)}$; and $E_{LUMO} = E_{HOMO}–Eg$ [58]. The value of the RhB HOMO-LUMO energy gap is 2.24 eV, and thus the energy of the LUMO is −3.79 eV.

From the positions of the energy band edges of the catalyst and pollutant (Fig. 5d), the feasibility of photocatalysis application can be predicted. When the valence band of the catalyst is higher in energy than the HOMO of the organic pollutant, the photodegradation process can occur, as the pollutant is oxidized by photogenerated holes in the catalyst surface [59]. As seen in Fig. 6d, the alignment of bands is suitable for photodegradation of RhB using heterojunction film; where the valence band of the heterojunction film is above (in the RHE scale) the HOMO of RhB, the photogenerated holes can directly oxidize the RhB molecule. The potential of the valence band edge of the semiconductors can also oxidize water, assisting the formation of intermediate species such as hydroxyl radicals and increasing the photocatalytic activity [60].

3.4. Photoelectrocatalytic activity

The photocatalytic properties of ZnO and $CuWO_4$ were compared to those of heterojunction films. These studies were performed under the following conditions: (i) photolysis (in the absence of any semiconductor), (ii) photocatalysis, and (iii) photoelectrocatalysis or electrochemically assisted photocatalysis (PEC). For these studies, an aqueous solution of RhB dye was used, and the results are shown in Fig. 6. Fig. 6a and c show the RhB degradation curves and kinetic curves (PEC configuration), respectively. Fig. 6b compares the photocatalytic activity of PC, PEC, and RhB photolysis. For Fig. 6a, the first 30 min of degradation were performed in the absence of irradiation to obtain adsorption equilibrium on the semiconductor surface. After the adsorption/desorption equilibrium period, the system was irradiated and the resulting decrease in RhB concentration was related to the photocatalysis process, in which the RhB dye was oxidized by photogenerated oxidant species [61]. Fig. 6b shows the degradation efficiency of the films. In the absence of a catalyst, the dye photolysis was approximately 10 %. Under PC conditions, the $CuWO_4$, ZnO and ZnO/$CuWO_4$ films presented a degradation efficiency of 35 %, 35 %, and 14 %, respectively, whereas under PEC conditions, the degradation efficiency was 46 %, 45 %, and 82 %, respectively. The photocatalytic degradation followed first-order kinetics [62] and the adjustment for PEC conditions is shown in Fig. 7b. Fig. 6c shows that the degradation PEC rate constant of ZnO/$CuWO_4$ heterojunction film was 7.86×10^{-3} min^{-1}, which is approximately threefold larger than the 2.75×10^{-3} min^{-1} rate constant of pure ZnO film. The heterojunction film had the highest degradation efficiency and a better kinetic profile. The kinetic rate constants of the PC, PEC, and photolysis processes are summarized in Table 1.

The degradation efficiency for the electrochemically assisted system is improved, which is expected because semiconductor photocatalytic activity and e^-/h^+ pairs recombination limiting factors [63,64]. The application of an external potential between the electrodes assists in the charge separation process, consequently delaying the recombination process [65,66].

Photoelectrochemical characterization and RhB degradation results showed that the ZnO/$CuWO_4$ heterojunction film possesses a higher activity than that of individual oxide films, especially under PEC

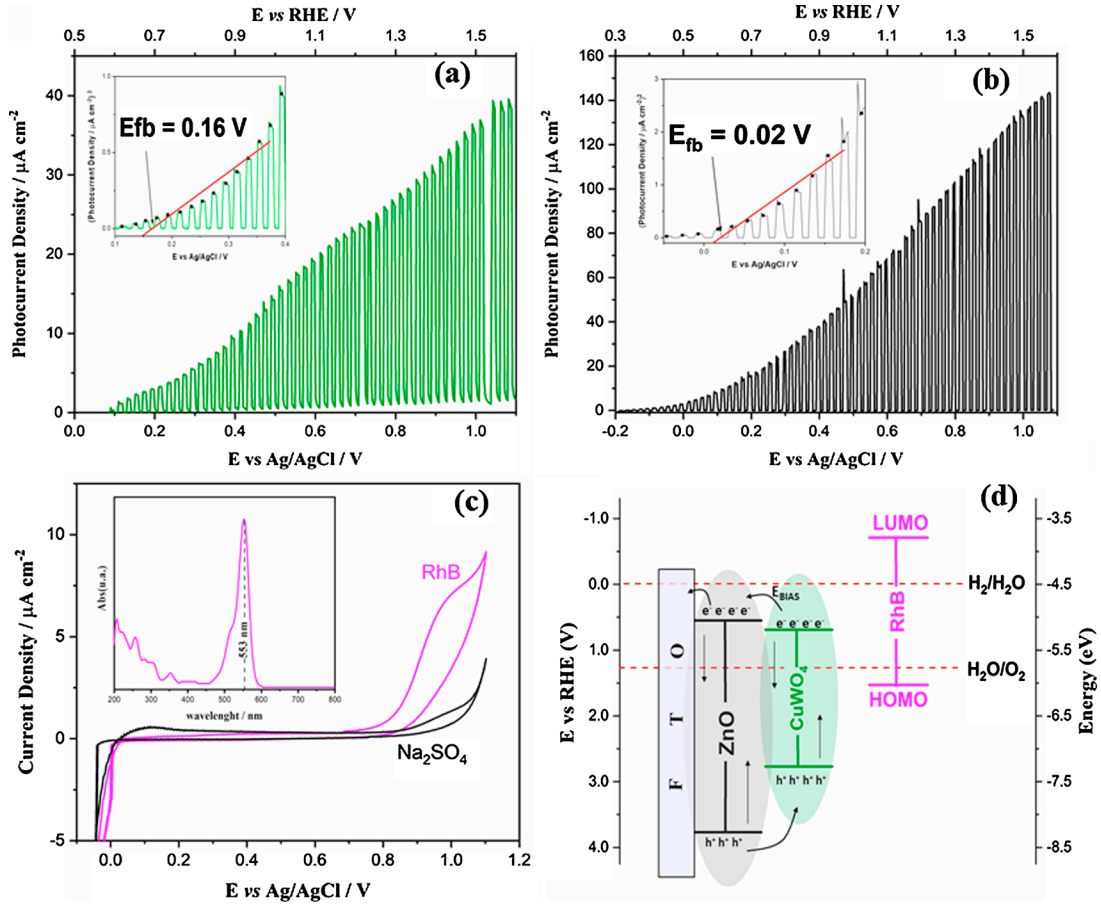

Fig. 5. Linear sweep voltammetry of (a) $CuWO_4$ and (b) ZnO films in 0.1 M Na_2SO_4 in the dark and under visible light illumination (*Inset*: corresponding curves de I^2 *vs* E used for determination at E_{FB}). (c) Cyclic voltammetry curve for RhB solution (Inset: UV–vis RhB absorbance spectra) and (d) energy diagram for the semiconductors/rhodamine-B interface in aqueous solution.

conditions, which can be attributed to better light absorption and an improvement in photogenerated charge transport between semiconductor bands under a bias external potential. Under PC conditions, as the conduction band (CB) of ZnO is more negative than that of $CuWO_4$, the photogenerated electrons do not flow in the direction of the substrate, favoring the recombination process and, thus, drastically reducing the photocatalytic activity. Under PEC conditions, the voltage applied at 0.7 V *vs* Ag/AgCl provides potential energy for the photogenerated electrons in the $CuWO_4$ CB to flow toward the ZnO CB in bulk and be collected by the system. Meanwhile, the holes flow toward the semiconductor/electrolyte interface and can directly oxidize the dye or cause indirect oxidation through the generation of oxidizing species such as the hydroxyl radical.

The PEC reusability of the heterojunction and ZnO was evaluated by reusing the film to photocatalyze RhB dye for five cycles (Fig. 7). Acceptable efficiency was observed after five cycles of reuse; therefore, the association with $CuWO_4$ conferred good stability to the ZnO/$CuWO_4$ heterojunction, and this result corroborates the previously discussed findings.

4. Conclusions

In this work, we successfully fabricated heterojunction nanostructured ZnO/$CuWO_4$ film electrodes onto an FTO conductive substrate. In the first step, the ZnO nanorods were synthesized using the hydrothermal method. In addition, $CuWO_4$ was synthesized using the co-precipitation/hydrothermal method and deposited onto ZnO nanorods *via* a doctor blade. From structural and morphological characterizations, it was observed that the top surface of wurtzite zinc oxide nanorods was covered by triclinic copper tungstate nanoparticles. The optical and photoelectrochemical results indicated that the covering of $CuWO_4$ on ZnO enhanced absorption of the film in the visible region, improved the photoelectrochemical activity of the ZnO film, and enhanced the photocorrosion stability. The photocatalytic activity for degradation of RhB solution under polychromatic irradiation presents better efficiency for ZnO/$CuWO_4$ film than for pure films, especially under a bias condition (PEC). The higher efficiency can be attributed to efficient charge separation and suppression of the recombination of e^-/h^+ pairs, thereby facilitating charge transfer.

CRediT authorship contribution statement

João P.C. Moura: Conceptualization, Methodology, Formal analysis, Investigation, Data curation, Writing - original draft, Writing - review & editing, Visualization. **Roberta Y.N. Reis:** Methodology, Investigation. **Aline E.B. Lima:** Resources, Methodology, Investigation. **Reginaldo S. Santos:** Conceptualization, Writing - review & editing. **Geraldo E. Luz:** Conceptualization, Methodology, Writing - review & editing, Supervision, Project administration.

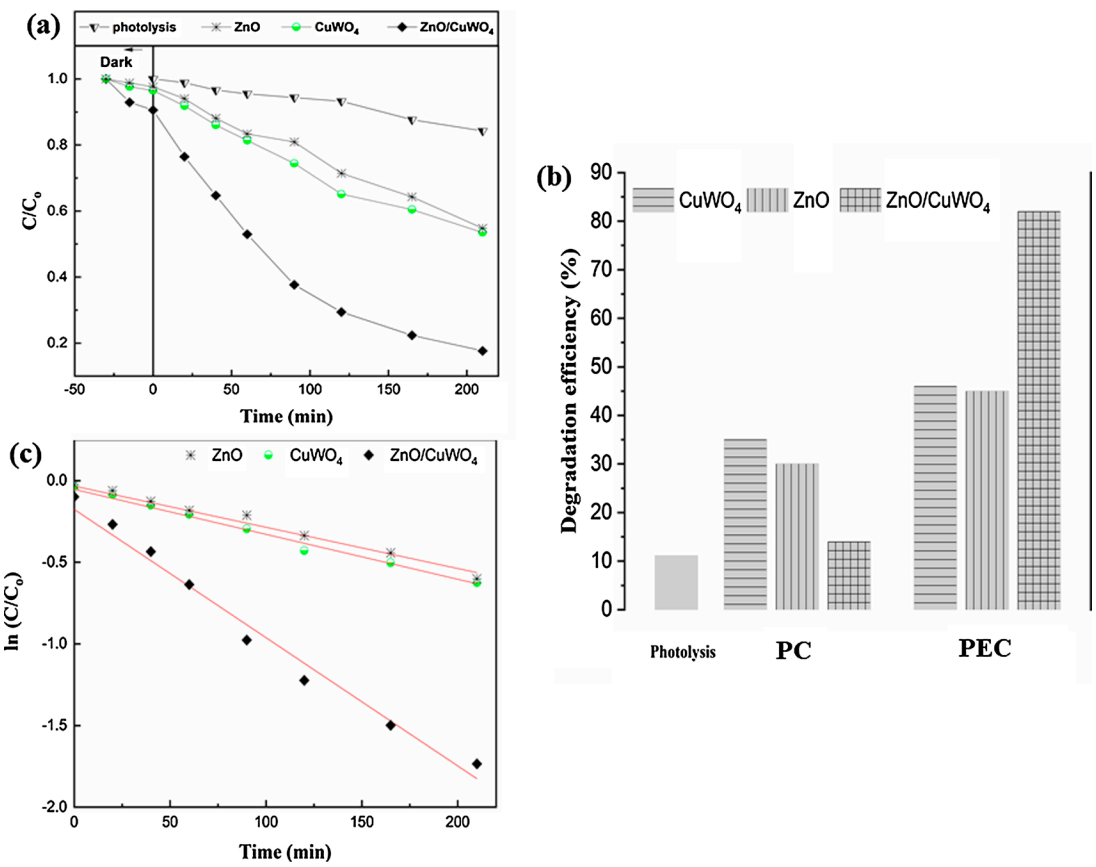

Fig. 6. (a) PEC RhB degradation activities of ZnO, $CuWO_4$, ZnO/$CuWO_4$ films under polychromatic light irradiation, (b) efficiency of degradation of films in different conditions (c) kinetic profiles of photodegradation.

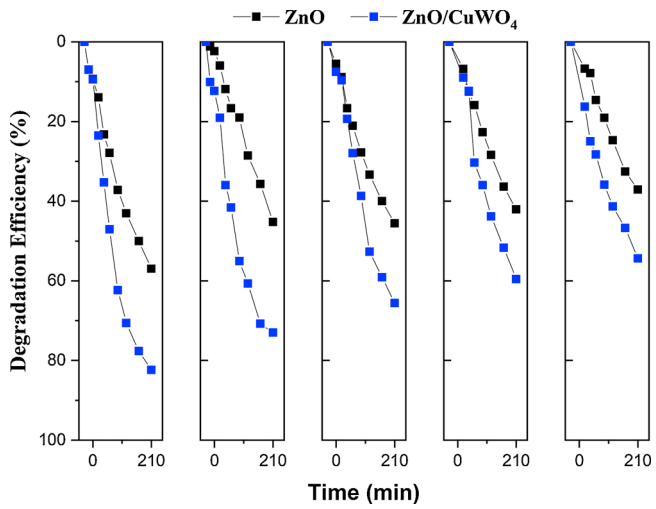

Fig. 7. Reusability efficiency of the ZnO/CuWO4 and ZnO films for EPC degradation of RhB.

Declaration of Competing Interest

The authors declare that they have no known competing financial interests or personal relationships that could have appeared to influence the work reported in this paper.

Table 1
Kinetic parameters of the RhB degradation in the different photocatalytic processes.

Photocatalyst	Photocatalytic Process	K (min^{-1})
–	Photolysis	$8.4 \times 10-4$
ZnO	PC	$1.4 \times 10-3$
	PEC	$2.7 \times 10-3$
$CuWO_4$	PC	$1.9 \times 10-3$
	PEC	$2.5 \times 10-3$
ZnO/$CuWO_4$	PC	$6.7 \times 10-4$
	PEC	$7.8 \times 10-3$

Acknowledgements

This work was funded by the following grants – CNPq (307559/2016-8, 305757/2018-0). The authors also wish to acknowledge financial support from the CAPES Institution.

References

[1] R. Marschall, Semiconductor composites: strategies for enhancing charge carrier separation to improve photocatalytic activity, Adv. Funct. Mater. 24 (2014) 2421–2440, https://doi.org/10.1002/adfm.201303214.
[2] S. Kumar, K. Ojha, A.K. Ganguli, Interfacial charge transfer in photoelectrochemical processes, Adv. Mater. Interfaces 4 (2017), https://doi.org/10.1002/admi.201600981.
[3] S. Varnagiris, A. Medvids, M. Lelis, D. Milcius, A. Antuzevics, Black carbon-doped TiO_2 films: synthesis, characterization and photocatalysis, J. Photochem. Photobiol. A: Chem. 382 (2019) 111941, , https://doi.org/10.1016/j.jphotochem.2019.

111941.
[4] P. Dash, A. Manna, N.C. Mishra, S. Varma, Synthesis and characterization of aligned ZnO nanorods for visible light photocatalysis, Physica E 107 (2019) 38–46, https://doi.org/10.1016/j.physe.2018.11.007.
[5] T. Xie, T. Zheng, R. Wang, T. Pu, X. Li, Y. Bu, J.P. Ao, A promising CuO_x/WO_3 p-n heterojunction thin-film photocathode fabricated by magnetron reactive sputtering, Int. J. Hydrogen Energy 44 (2019) 4062–4071, https://doi.org/10.1016/j.ijhydene.2018.12.153.
[6] W. Ding, X. Wu, Q. Lu, Structure and photocatalytic activity of thin-walled $CuWO_4$ nanotubes: an experimental and DFT study, Mater. Lett. 253 (2019) 323–326, https://doi.org/10.1016/j.matlet.2019.06.109.
[7] R. Venkatesan, S. Velumani, K. Ordon, M. Makowska-Janusik, G. Corbel, A. Kassiba, Nanostructured bismuth vanadate ($BiVO_4$) thin films for efficient visible light photocatalysis, Mater. Chem. Phys. 205 (2018) 325–333, https://doi.org/10.1016/j.matchemphys.2017.11.004.
[8] Q. Zhang, Y. Huang, S. Peng, Y. Zhang, Z. Shen, Jji Cao, W. Ho, S.C. Lee, D.Y.H. Pui, Perovskite $LaFeO_3$-$SrTiO_3$ composite for synergistically enhanced NO removal under visible light excitation, Appl. Catal. B Environ. 204 (2017) 346–357, https://doi.org/10.1016/j.apcatb.2016.11.052.
[9] M. Pirhashemi, A. Habibi-Yangjeh, S. Rahim Pouran, Review on the criteria anticipated for the fabrication of highly efficient ZnO-based visible-light-driven photocatalysts, J. Ind. Eng. Chem. 62 (2018) 1–25, https://doi.org/10.1016/j.jiec.2018.01.012.
[10] S.J.A. Moniz, S.A. Shevlin, D.J. Martin, Z.X. Guo, J. Tang, Visible-light driven heterojunction photocatalysts for water splitting-a critical review, Energy Environ. Sci. 8 (2015) 731–759, https://doi.org/10.1039/c4ee03271c.
[11] S. Zhao, Y. Zhang, Y. Zhou, C. Zhang, J. Fang, X. Sheng, Ionic liquid-assisted photochemical synthesis of ZnO/Ag_2O heterostructures with enhanced visible light photocatalytic activity, Appl. Surf. Sci. 410 (2017) 344–353, https://doi.org/10.1016/j.apsusc.2017.03.051.
[12] A. Baranowska-Korczyc, M. Kościński, E.L. Coy, B.F. Grześkowiak, M. Jasiurkowska-Delaporte, B. Peplińska, S. Jurga, ZnS coating for enhanced environmental stability and improved properties of ZnO thin films, RSC Adv. 8 (2018) 24411–24421, https://doi.org/10.1039/c8ra02823k.
[13] V. Neshchimenko, C. Li, M. Mikhailov, J. Lv, Optical radiation stability of ZnO hollow particles, Nanoscale. 10 (2018) 22335–22347, https://doi.org/10.1039/c8nr04455d.
[14] A.E. Kandjani, Y.M. Sabri, S.R. Periasamy, N. Zohora, M.H. Amin, A. Nafady, S.K. Bhargava, Controlling core/shell formation of nanocubic p-Cu_2O/n-ZnO toward enhanced photocatalytic performance, Langmuir 31 (2015) 10922–10930, https://doi.org/10.1021/acs.langmuir.5b01019.
[15] A. Serrà, Y. Zhang, B. Sepúlveda, E. Gómez, J. Nogués, J. Michler, L. Philippe, Highly active ZnO-based biomimetic fern-like microleaves for photocatalytic water decontamination using sunlight, Appl. Catal. B Environ. 248 (2019) 129–146, https://doi.org/10.1016/j.apcatb.2019.02.017.
[16] J. Sen Chang, J. Strunk, M.N. Chong, P.E. Poh, J.D. Ocon, Multi-dimensional zinc oxide (ZnO) nanoarchitectures as efficient photocatalysts: what is the fundamental factor that determines photoactivity in ZnO, J. Hazard. Mater. 381 (2020) 120958, , https://doi.org/10.1016/j.jhazmat.2019.120958.
[17] Y.X. Wang, Z.C. Shen, D.D. Huang, Z.S. Yang, High-performance ZnO nanosheets/nanocrystalline aggregates composite photoanode film in dye-sensitized solar cells, Mater. Lett. 214 (2018) 88–90, https://doi.org/10.1016/j.matlet.2017.11.057.
[18] E. Muchuweni, T.S. Sathiaraj, H. Nyakotyo, Effect of annealing on the microstructural, optical and electrical properties of ZnO nanowires by hydrothermal synthesis for transparent electrode fabrication, Mater. Sci. Eng. B Solid-State Mater. Adv. Technol. 227 (2018) 68–73, https://doi.org/10.1016/j.mseb.2017.10.006.
[19] F.Y. Su, W. De Zhang, Fabrication and photoelectrochemical property of In_2O_3/ZnO composite nanotube arrays using ZnO nanorods as self-sacrificing templates, Mater. Lett. 211 (2018) 65–68, https://doi.org/10.1016/j.matlet.2017.09.085.
[20] L. Xu, J. Su, G. Zheng, L. Zhang, Enhanced photocatalytic performance of porous ZnO thin films by CuO nanoparticles surface modification, Mater. Sci. Eng. B Solid-State Mater. Adv. Technol. 248 (2019), https://doi.org/10.1016/j.mseb.2019.114405.
[21] F. Bouhjar, B. Marí, B. Bessaïs, Hydrothermal fabrication and characterization of ZnO/Fe_2O_3 heterojunction devices for hydrogen production, J. Anal. Pharm. Res. 7 (2018), https://doi.org/10.15406/japlr.2018.07.00246.
[22] Y.M. Hunge, M.A. Mahadik, A.V. Moholkar, C.H. Bhosale, Photoelectrocatalytic degradation of phthalic acid using spray deposited stratified WO_3/ZnO thin films under sunlight illumination, Appl. Surf. Sci. 420 (2017) 764–772, https://doi.org/10.1016/j.apsusc.2017.05.221.
[23] X. Huang, J. Song, L. Wang, X. Gu, Y. Zhao, Y. Qiang, Photoelectrochemical properties of ZnO/$BiVO_4$ nanorod arrays prepared through a facile spin-coating deposition route, Mater. Sci. Semicond. Process. 97 (2019) 106–111, https://doi.org/10.1016/j.mssp.2019.03.019.
[24] R. Salimi, A.A. Sabbagh Alvani, B.T. Mei, N. Naseri, S.F. Du, G. Mul, Ag-Functionalized $CuWO_4/WO_3$ nanocomposites for solar water splitting, New J. Chem. 43 (2019) 2196–2203, https://doi.org/10.1039/c8nj05625k.
[25] J.C. Hill, K.S. Choi, Synthesis and characterization of high surface area $CuWO_4$ and Bi_2WO_6 electrodes for use as photoanodes for solar water oxidation, J. Mater. Chem. A. 1 (2013) 5006–5014, https://doi.org/10.1039/c3ta10245a.
[26] A. Habibi-Yangjeh, M. Mousavi, Deposition of $CuWO_4$ nanoparticles over g-C_3N_4 /Fe_3O_4 nanocomposite: novel magnetic photocatalysts with drastically enhanced performance under visible-light, Adv. Powder Technol. 29 (2018) 1379–1392, https://doi.org/10.1016/j.apt.2018.02.034.
[27] D. Roy, G.F. Samu, M.K. Hossain, C. Janáky, K. Rajeshwar, On the measured optical bandgap values of inorganic oxide semiconductors for solar fuels generation, Catal. Today 300 (2018) 136–144, https://doi.org/10.1016/j.cattod.2017.03.016.
[28] A. Thomas, C. Janáky, G.F. Samu, M.N. Huda, P. Sarker, J.P. Liu, V. Van Nguyen, E.H. Wang, K.A. Schug, K. Rajeshwar, Time- and energy-efficient solution combustion synthesis of binary metal tungstate nanoparticles with enhanced photocatalytic activity, ChemSusChem. 8 (2015) 1652–1663, https://doi.org/10.1002/cssc.201500383.
[29] J.E. Yourey, B.M. Bartlett, Electrochemical deposition and photoelectrochemistry of $CuWO_4$, a promising photoanode for water oxidation, J. Mater. Chem. 21 (2011) 7651–7660, https://doi.org/10.1039/c1jm11259g.
[30] M. Joseita dos Santos Costa, G. dos Santos Costa, A. Estefany Brandão Lima, G. Eduardo da Luz Júnior, E. Longo, L. Santos Cavalcante, R. da Silva Santos, Photocurrent response and progesterone degradation by employing WO_3 films modified with platinum and silver nanoparticles, Chempluschem 83 (2018) 1153–1161, https://doi.org/10.1002/cplu.201800534.
[31] D. Cao, Y. Wang, M. Qiao, X. Zhao, Enhanced photoelectrocatalytic degradation of norfloxacin by an Ag_3PO_4/$BiVO_4$ electrode with low bias, J. Catal. 360 (2018) 240–249, https://doi.org/10.1016/j.jcat.2018.01.017.
[32] S. Garcia-Segura, E. Brillas, Applied photoelectrocatalysis on the degradation of organic pollutants in wastewaters, J. Photochem. Photobiol. C Photochem. Rev. 31 (2017) 1–35, https://doi.org/10.1016/j.jphotochemrev.2017.01.005.
[33] M. Shekofteh-Gohari, A. Habibi-Yangjeh, Fabrication of novel magnetically separable visible-light-driven photocatalysts through photosensitization of Fe_3O_4/ZnO with $CuWO_4$, J. Ind. Eng. Chem. 44 (2016) 174–184, https://doi.org/10.1016/j.jiec.2016.08.028.
[34] T. Mavrič, M. Valant, M. Forster, A.J. Cowan, U. Lavrenčič, S. Emin, Design of a highly photocatalytically active ZnO/$CuWO_4$ nanocomposite, J. Colloid Interface Sci. 483 (2016) 93–101, https://doi.org/10.1016/j.jcis.2016.08.019.
[35] F. Zhou, X. Li, J. Shu, J. Wang, Synthesis and visible light photo-electrochemical behaviors of In_2O_3-sensitized ZnO nanowire array film, J. Photochem. Photobiol. A: Chem. 219 (2011) 132–138, https://doi.org/10.1016/j.jphotochem.2011.02.002.
[36] A.E.B. Lima, M.J.S. Costa, R.S. Santos, N.C. Batista, L.S. Cavalcante, E. Longo, G.E. Luz, Facile preparation of $CuWO_4$ porous films and their photoelectrochemical properties, Electrochim. Acta 256 (2017) 139–145, https://doi.org/10.1016/j.electacta.2017.10.010.
[37] I. Rodríguez-Gutiérrez, E. Djatoubai, M. Rodríguez-Pérez, J. Su, G. Rodríguez-Gattorno, L. Vayssieres, G. Oskam, Photoelectrochemical water oxidation at FTO|WO_3@$CuWO_4$ and FTO|WO_3@$CuWO_4$|$BiVO_4$ heterojunction systems: an IMPS analysis, Electrochim. Acta 308 (2019) 317–327, https://doi.org/10.1016/j.electacta.2019.04.030.
[38] S.C. Abrahams, J.L. Bernstein, Remeasurement of the structure of hexagonal ZnO, acta crystallogr, Sect. B Struct. Crystallogr. Cryst. Chem. 25 (1969) 1233–1236, https://doi.org/10.1107/s0567740869003876.
[39] L. Kihlborg, E. Gebert, $CuWO_4$, a distorted Wolframite-type structure, Acta Crystallogr. Sect. B Struct. Crystallogr. Cryst. Chem. 26 (1970) 1020–1026, https://doi.org/10.1107/s0567740870003515.
[40] J.S. Yang, J.J. Wu, Low-potential driven fully-depleted $BiVO_4$/ZnO heterojunction nanodendrite array photoanodes for photoelectrochemical water splitting, Nano Energy 32 (2017) 232–240, https://doi.org/10.1016/j.nanoen.2016.12.039.
[41] D.L. Wood, 0. 05-0. 08, Phys. Rev. B 5 (1972) 3144–3151.
[42] K. Ahmadi, A. Abdolahzadeh Ziabari, K. Mirabbaszadeh, S. Ahmadi, Synthesis of TiO_2 nanotube array thin films and determination of the optical constants using transmittance data, Superlattices Microstruct. 77 (2015) 25–34, https://doi.org/10.1016/j.spmi.2014.10.024.
[43] E.L.S. Souza, C.J. Dalmaschio, M.G.R. Filho, G.E.L. Jr, R.S. Santos, E. Longo, Structural refinement and photocatalytic properties of $CuWO_4$ crystals, Microsc. Adv. Sci. Res. Educ. (2014) 894–902.
[44] R. Lei, H. Zhang, H. Ni, R. Chen, H. Gu, B. Zhang, Novel ZnO nanoparticles modified WO_3 nanosheet arrays for enhanced photocatalytic properties under solar light illumination, Appl. Surf. Sci. 463 (2019) 363–373, https://doi.org/10.1016/j.apsusc.2018.08.218.
[45] M. Zhang, C. Yang, W. Pu, Y. Tan, K. Yang, J. Zhang, Liquid phase deposition of WO_3/TiO_2 heterojunction films with high photoelectrocatalytic activity under visible light irradiation, Electrochim. Acta 148 (2014) 180–186, https://doi.org/10.1016/j.electacta.2014.10.043.
[46] G.S. Costa, M.J.S. Costa, H.G. Oliveira, L.C.B. Lima, G.E. Luz, L.S. Cavalcante, R.S. Santos, Effect of the applied potential condition on the photocatalytic properties of Fe_2O_3|WO_3 heterojunction films, J. Inorg. Organomet. Polym. Mater. (2020), https://doi.org/10.1007/s10904-019-01429-0.
[47] I. Gonzalez-Valls, M. Lira-Cantu, Vertically-aligned nanostructures of ZnO for excitonic solar cells: a review, Energy Environ. Sci. 2 (2009) 19–34, https://doi.org/10.1039/b811536b.
[48] J. Ai, C. Lin, W. Liao, C. Hu, T. Zhou, S. Luo, L. Cheng, Z. Chen, Y. Yang, Y. Zhang, W. Li, Shape-controlled synthesis of bare ZnO nanomaterials with improved photoactivity and photostability, Mater. Sci. Technol. (United Kingdom) 35 (2019) 336–348, https://doi.org/10.1080/02670836.2018.1558578.
[49] M. Zhou, Z. Liu, X. Li, Z. Liu, Promising three-dimensional flowerlike $CuWO_4$ photoanode modified with CdS and FeOOH for efficient photoelectrochemical water splitting, Ind. Eng. Chem. Res. 57 (2018) 6210–6217, https://doi.org/10.1021/acs.iecr.8b00358.
[50] H. Yan, J. Hou, Z. Fu, B. Yang, P. Yang, K. Liu, M. Wen, Y. Chen, S. Fu, F. Li, Growth and photocatalytic properties of one-dimensional ZnO nanostructures prepared by thermal evaporation, Mater. Res. Bull. 44 (2009) 1954–1958, https://doi.org/10.1016/j.materresbull.2009.06.014.
[51] M.A. Butler, Photoelectrolysis and physical properties of the semiconducting electrode WO_2, J. Appl. Phys. 48 (1977) 1914–1920, https://doi.org/10.1063/1.323948.

[52] M. Hepel, S. Hazelton, Photoelectrocatalytic degradation of diazo dyes on nanostructured WO_3 electrodes, Electrochim. Acta 50 (2005) 5278–5291, https://doi.org/10.1016/j.electacta.2005.03.067.
[53] M.A. Alpuche-Aviles, Y. Wu, Photoelectrochemical study of the band structure of Zn_2SnO_4 prepared by the hydrothermal method, J. Am. Chem. Soc. 131 (2009) 3216–3224, https://doi.org/10.1021/ja806719x.
[54] Q. He, J. Liu, Y. Tian, Y. Wu, F. Magesa, P. Deng, G. Li, Facile preparation of Cu_2O nanoparticles and reduced graphene oxide nanocomposite for electrochemical sensing of rhodamine B, Nanomaterials 9 (2019) 958, https://doi.org/10.3390/nano9070958.
[55] Q. He, J. Liu, Y. Xia, D. Tuo, P. Deng, Y. Tian, Y. Wu, G. Li, D. Chen, Rapid and sensitive voltammetric detection of rhodamine B in chili-containing foodstuffs using mno_2nanorods/electro-reduced graphene oxide composite, J. Electrochem. Soc. 166 (2019) B805–B813, https://doi.org/10.1149/2.1271910jes.
[56] C.M. Cardona, W. Li, A.E. Kaifer, D. Stockdale, G.C. Bazan, Electrochemical considerations for determining absolute frontier orbital energy levels of conjugated polymers for solar cell applications, Adv. Mater. 23 (2011) 2367–2371, https://doi.org/10.1002/adma.201004554.
[57] L. Leonat, G. Sbârcea, I.V. Brañzoi, Cyclic voltammetry for energy levels estimation of organic materials, UPB Sci. Bull. Ser. B Chem. Mater. Sci. 75 (2013) 111–118.
[58] Y. Li, Y. Li, Y. Chu, X. Tao, H. Xu, Y. Shen, A. Zheng, An experimental and quantum mechanical study on luminescence properties of $SM(\beta\text{-}Nbm)_3$·(Pd), J. Lumin. 132 (2012) 1663–1667, https://doi.org/10.1016/j.jlumin.2012.02.023.
[59] X. Xiao, S. Tu, M. Lu, H. Zhong, C. Zheng, X. Zuo, J. Nan, Discussion on the reaction mechanism of the photocatalytic degradation of organic contaminants from a viewpoint of semiconductor photo-induced electrocatalysis, Appl. Catal. B Environ. 198 (2016) 124–132, https://doi.org/10.1016/j.apcatb.2016.05.042.
[60] G. Zheng, J. Wang, H. Liu, V. Murugadoss, G. Zu, H. Che, C. Lai, H. Li, T. Ding, Q. Gao, Z. Guo, Tungsten oxide nanostructures and nanocomposites for photoelectrochemical water splitting, Nanoscale. (2019), https://doi.org/10.1039/c9nr03474a.
[61] B. Srikanth, R. Goutham, R. Badri Narayan, A. Ramprasath, K.P. Gopinath, A.R. Sankaranarayanan, Recent advancements in supporting materials for immobilised photocatalytic applications in waste water treatment, J. Environ. Manage. 200 (2017) 60–78, https://doi.org/10.1016/j.jenvman.2017.05.063.
[62] M.H. Barzegar, M. Ghaedi, V. Madadi Avargani, M.M. Sabzehmeidani, F. Sadeghfar, R. Jannesar, Electrochemical synthesis of Zn:ZnO/Ni_2P and efficient photocatalytic degradation of Auramine O in aqueous solution under multi-variable experimental design optimization, Polyhedron. 165 (2019) 1–8, https://doi.org/10.1016/j.poly.2019.02.003.
[63] A.B.K. dos Santos, E.M.T. Claro, R.N. Montagnolli, J.M. Cruz, P.R.M. Lopes, E.D. Bidoia, Electrochemically assisted photocatalysis: highly efficient treatment using thermal titanium oxides doped and non-doped electrodes for water disinfection, J. Environ. Manage. 204 (2017) 255–263, https://doi.org/10.1016/j.jenvman.2017.09.006.
[64] J. Wu, H. Xu, W. Yan, Photoelectrocatalytic degradation Rhodamine B over highly ordered TiO_2 nanotube arrays photoelectrode, Appl. Surf. Sci. 386 (2016) 1–13, https://doi.org/10.1016/j.apsusc.2016.05.155.
[65] M.J.S. Costa, G.S. Costa, A.E.B. Lima, G.E. Luz, E. Longo, L.S. Cavalcante, R.S. Santos, Investigation of charge recombination lifetime in γ-WO_3 films modified with Ag^* and Pt^* nanoparticles and its influence on photocurrent density, Ionics (Kiel). 24 (2018) 3291–3297, https://doi.org/10.1007/s11581-018-2640-1.
[66] M.G. Peleyeju, O.A. Arotiba, Recent trend in visible-light photoelectrocatalytic systems for degradation of organic contaminants in water/wastewater, Environ. Sci. Water Res. Technol. 4 (2018) 1389–1411, https://doi.org/10.1039/c8ew00276b.